

Solar-Blind AlGa_N Heterostructure Photodiodes

J.D. Brown¹, Jizhong Li¹, P. Srinivasan¹, J. Matthews¹ and J.F. Schetzina¹

¹Department of Physics, North Carolina State University,

(Received Friday, August 11, 2000; accepted Wednesday, September 13, 2000)

A backside-illuminated solar-blind UV detector based on an AlGa_N p-i-n heterostructure has been successfully synthesized, fabricated and tested. The p-i-n photodiode structure consists of a 1.0 μm n-type Al_{0.64}Ga_{0.36}N:Si layer grown by MOVPE onto a low temperature AlN buffer layer on a polished sapphire substrate. On top of this base layer is a 0.2 μm undoped Al_{0.47}Ga_{0.53}N active layer and a 0.5 μm p-type Al_{0.47}Ga_{0.53}N:Mg top layer. Square mesas of area $A = 4 \times 10^{-4} \text{ cm}^2$ were obtained by reactive ion etching using BCl₃. The solar-blind photodiode exhibits a very narrow UV spectral responsivity band peaked at 273 nm with a FWHM = 21 nm. Maximum responsivity $R = 0.051 \text{ A/W}$ at 273 nm, corresponding to an internal quantum efficiency of 27%. R_0A values up to $8 \times 10^7 \Omega\text{-cm}^2$ were obtained, corresponding to $D^* = 3.5 \times 10^{12} \text{ cm Hz}^{1/2} \text{ W}^{-1}$ at 273 nm.

1 Introduction

Atmospheric absorption of sunlight by ozone and oxygen gives rise to a narrow UV absorption band at the earth's surface from about 240-285 nm that is termed the "solar-blind" UV region [1] [2]. UV detectors that respond exclusively to radiation in this wavelength region are termed "solar-blind" detectors since they can detect objects that emit radiation in this narrow wavelength window without interference from the sun — provided that both the detector and the object of interest are at or near the surface of the earth. Solar-blind detectors are to be distinguished from "visible-blind" UV detectors and detector arrays that have UV responsivity bands outside of the solar-blind window but remain blind to visible radiation. Visible-blind UV detectors and detector arrays based on III-V nitride structures have been reported in a number of recent publications [2] [3] [4] [5] [6] [7] [8] [9] [10]

This paper reports the successful synthesis, fabrication, and testing of a backside-illuminated solar-blind UV detector based on an AlGa_N p-i-n heterostructure. The structure of the device is first described. This is followed by a description of the experimental procedures employed to synthesize and characterize the various layers of the heterostructure. Processing procedures employed to prepare discrete 200 μm x 200 μm mesa photodiodes are next described. This is followed by a discussion of the device characteristics obtained from

spectral responsivity and R_0A measurements from which the photodiode detectivity D^* was estimated.

2 Experimental Details

2.1 Photodiode Structure

Photodiode structures were prepared by MOVPE at North Carolina State University using a low-pressure, vertical-flow reactor that employs high speed substrate rotation during film growth [6] [7] [8]. The photodiode structures were deposited onto 2 inch diameter c-plane sapphire substrates. A thin (~30 nm) AlN buffer layer was deposited at 500-650 °C to initiate growth; all subsequent layers were grown at 1105 °C.

A schematic of the photodiode structure employed in the present work is shown in Figure 1. The thin low temperature AlN nucleation layer is first deposited followed by a ~1.0 μm thick n-type silicon doped Al_{0.64}Ga_{0.36}N:Si base layer. An undoped 0.2 μm thick Al_{0.47}Ga_{0.53}N active layer is then deposited followed by a 0.5 μm thick p-type magnesium doped Al_{0.47}Ga_{0.53}N:Mg layer to complete the p-i-n heterostructure. Note that this device structure is designed for through-the-substrate illumination. The photodiode structure shown in Figure 1 is designed to respond to UV light in the wavelength band from about 250 nm to 285 nm. At wavelengths shorter than 250 nm, the incoming light is absorbed in the thick AlGa_N base layer (~64% Al) and the junction is not illuminated. Likewise, the diode does not respond to wavelengths

greater than 285 nm, since this corresponds to the optical absorption edge of $\text{Al}_{0.47}\text{Ga}_{0.53}\text{N}$ at 300K.

In order to optimize the above photodiode structure, a series of samples were grown under various combinations of growth temperatures, growth rates, and gas flow rates. First, the n-type $\text{Al}_{0.64}\text{Ga}_{0.36}\text{N}:\text{Si}$ was optimized. Capacitance-voltage (C-V), optical absorption, and cathodoluminescence (CL) measurements were employed in this optimization procedure. The undoped $\text{Al}_{0.47}\text{Ga}_{0.53}\text{N}$ active layer and p-type magnesium doped $\text{Al}_{0.47}\text{Ga}_{0.53}\text{N}:\text{Mg}$ top layer of the device structure were then optimized with the aid of optical absorption and cathodoluminescence measurements.

2.2 Device Processing

All device processing was completed using standard semiconductor processing techniques which included photolithography using appropriately-designed masks, reactive ion etching to define mesa structures, and metallizations to provide ohmic contacts to the n-type and p-type layers of the devices. Boron trichloride (BCl_3) was employed in the reactive ion etching chamber using photolithographically defined Ni masks to etch the $200\ \mu\text{m} \times 200\ \mu\text{m}$ photodiode mesas. Etch rates of ~ 17.5 nm/sec were obtained using BCl_3 flow rates of 35 sccm at a chamber pressure of 30 mTorr and an RF power level of 100 W. Ni/Au and Ti/Al metallizations, followed by an anneal at 600-700 °C, were employed to obtain p-type and n-type ohmic contacts, respectively.

2.3 Device Testing

Spectral responsivity measurements were completed on selected photodiode samples. In these experiments, a xenon lamp was employed as a UV source and the UV wavelengths were selected by a monochromator. The monochromator output was calibrated using a calibrated UV-enhanced Si photodiode. The detector current responsivity R_λ is defined as the output current i_p produced by the detector divided by the diode illumination power P_λ at a given wavelength λ . That is,

$$R_\lambda = i_p/P_\lambda = q\eta/h\nu \quad (\text{A/W}) \quad (1)$$

where q is the electronic charge, η is the external quantum efficiency, h is Planck's constant and ν is the radiation frequency [11]. Note that the responsivity R_λ varies inversely with the optical frequency ν . As a consequence, maximum responsivities ($\eta = 1$) in the UV are small — ranging from $R_\lambda = 0.294$ A/W at 365 nm to $R_\lambda = 0.161$ A/W at 200 nm.

The 300K dynamic resistance of the photodiode at zero-bias R_0 was measured for selected devices using a shielded low-noise enclosure and shielded probe tips.

These measurements were combined with the device area A to obtain the R_0A product — a well-known photodiode figure of merit. The R_0A product was then used to obtain an estimate of the noise-limited detector detectivity D^* .

The spectral detectivity D^* of a photodiode detector may be expressed as [11]

$$D^* = (q\eta/h\nu) [(4kT/R_0A) + 2q^2\eta\Phi_b]^{-1/2} \quad (\text{cm Hz}^{1/2}\text{W}^{-1}). \quad (2)$$

The first term in the bracketed quantity above ($4kT/R_0A$) arises from thermal noise sources within the detector. The second term ($2q^2\eta\Phi_b$) is due to the background radiation Φ_b to which the detector is exposed. If the detector is limited by thermal noise, that is, if the thermal noise far exceeds the background-radiation-induced signal, then the detectivity may be expressed as

$$D^* = (q\eta/h\nu) [(4kT/R_0A)]^{-1/2} = R_\lambda (R_0A/4kT)^{1/2} \quad (\text{cm Hz}^{1/2}\text{W}^{-1}), \quad (3)$$

where k is Boltzmann's constant and T is the absolute temperature. Note that the detectivity D^* is directly proportional to $(R_0A)^{1/2}$ when the detector is noise-limited. In the present work, Equation (3) was used to estimate D^* .

3 Results and Discussion

3.1 Characterization of $\text{Al}_x\text{Ga}_{1-x}\text{N}$ Layers

Figure 2 shows cathodoluminescence (CL) spectra obtained during the device optimization process for three different $\text{Al}_{0.64}\text{Ga}_{0.36}\text{N}:\text{Si}$ base layers. Figure 2a was obtained for an early sample that was not optimized — and which displayed a rough surface texture. Note that the spectrum for this sample is dominated by deep level emissions. Specifically, there is a broad peak centered at about 500 nm that may be related to the Si doping process. In addition, there is a peak at 319 nm that, we believe, is defect related and may occur due to the presence of small localized regions within the sample that contain less Al than expected. The sharper peak at 250 nm is the near band edge peak associated with an AlGa_N alloy having approximately 64% Al. Figure 2b shows CL from an improved $\text{Al}_{0.64}\text{Ga}_{0.36}\text{N}:\text{Si}$ base layer. In this case the spectrum is dominated by a near band edge peak at 247 nm and a diminished deep level broad emission. However, the defect related peak at 315 nm is still present in the spectrum. Figure 2c shows CL from an optimized $\text{Al}_{0.64}\text{Ga}_{0.36}\text{N}:\text{Si}$ base layer. In this case, the CL spectrum contains a strong near band edge peak at 247 nm and a broad deep level peak associated with the Si doping process. Note, however, that the

defect related peak that occurs at about 315-319 nm is absent from this spectrum. We have found that the absence of the 315-319 nm CL peak in the $\text{Al}_{0.64}\text{Ga}_{0.36}\text{N}:\text{Si}$ base layer is necessary for the finished photodiode device to exhibit a large and narrow UV responsivity curve. Note, also, that the broad deep level emission peak moves from about 500 nm to 430 nm for the optimized $\text{Al}_{0.64}\text{Ga}_{0.36}\text{N}:\text{Si}$ sample shown in Figure 2c.

Capacitance-voltage (C-V) measurements at low (1 KHz) and high (1 MHz) frequencies were performed in order to estimate the net donor density $N_d - N_a$ and the free carrier density, respectively [12] [13]. The low frequency capacitance should be dependent on the density of deep and shallow impurities $N_d - N_a$, while the high frequency capacitance depends on the free carrier density n [13]. From such measurements on the optimized $\text{Al}_{0.64}\text{Ga}_{0.36}\text{N}:\text{Si}$ base layer of Figure 2c one obtains $N_d - N_a \sim 1.0 \times 10^{18} \text{ cm}^{-3}$ and $n \sim 3.0 \times 10^{17} \text{ cm}^{-3}$. Low and high frequency C-V measurements on n-type GaN:Si samples generally give the same numerical result for $N_d - N_a$ and n , implying that the silicon donors are completely ionized at 300K. For the $\text{Al}_{0.64}\text{Ga}_{0.36}\text{N}:\text{Si}$ sample, however, the C-V results suggest that only about 30% of the Si donors are ionized at 300K. This result implies that the Si donor ionization energy is larger in AlGaN alloys. A detailed study of how the Si donor ionization energy varies with increasing Al content in AlGaN alloys is under investigation and will be reported at a later date.

Figure 3 shows CL spectra obtained for three different p-type magnesium doped $\text{Al}_{0.47}\text{Ga}_{0.53}\text{N}:\text{Mg}$ layers. These spectra were obtained from the top p-type layers of three different device structures grown under increasing Mg flow rate. After the depositions the p-type layers were activated with an 800 °C anneal under N_2 . Figure 3a shows the CL spectrum obtained for a lightly doped $\text{Al}_{0.47}\text{Ga}_{0.53}\text{N}:\text{Mg}$ layer. For this sample, the CL spectrum consists of a sharp near band edge peak at 275 nm and two broad deep level emissions. The peak centered at about 500 nm is most likely related to the presence of an unintentional n-type dopant, possibly oxygen; whereas, the peak centered at about 350 nm is believed to be associated with the Mg p-type doping process. This interpretation is consistent with the CL spectrum shown in Figure 3b, which was obtained for a moderately doped $\text{Al}_{0.47}\text{Ga}_{0.53}\text{N}:\text{Mg}$ layer. In this case, the spectrum contains a near band edge peak at 269 nm and a broad peak centered at 350 nm. The deeper emission peak at about 500 nm is absent from the spectrum. The CL spectrum for a more-heavily-doped sample is shown in Figure 3c. In this case, the spectrum contains

a single broad peak centered at 353 nm. It should be noted that the spectral changes reported here for $\text{Al}_{0.47}\text{Ga}_{0.53}\text{N}:\text{Mg}$ layers are similar to the changes that occur for GaN:Mg with increasing Mg content [14] — except the various emissions are shifted to shorter wavelengths for the $\text{Al}_{0.47}\text{Ga}_{0.53}\text{N}:\text{Mg}$ sample.

Meaningful C-V measurements could not be obtained for the $\text{Al}_{0.47}\text{Ga}_{0.53}\text{N}:\text{Mg}$ layers. However, for the most heavily doped AlGaN:Mg sample of Figure 3c, we estimate that the net acceptor concentration $N_a - N_d$ is about $5 \times 10^{19} \text{ cm}^{-3}$, assuming that the Mg incorporation process in AlGaN is the same as for GaN. Using high Mg doping levels in $\text{Al}_{0.47}\text{Ga}_{0.53}\text{N}:\text{Mg}$ layers, we have found that processed solar blind photodiodes which employ the device structure shown in Figure 1 generally exhibit high leakage currents under reverse bias conditions. For this reason, we employed $\text{Al}_{0.47}\text{Ga}_{0.53}\text{N}:\text{Mg}$ top layers with light to moderate Mg incorporation in the solar blind photodiodes reported in the present work. We estimate that the free hole density $p \leq 1.0 \times 10^{16} \text{ cm}^{-3}$ at 300K in these p-type layers.

Optical transmission spectra from 200 - 750 nm are shown in Figure 4. In Figure 4a, the transmittance obtained for an optimized 1.0 μm thick $\text{Al}_{0.64}\text{Ga}_{0.36}\text{N}:\text{Si}$ base layer is displayed. Regular interference oscillations are seen in the transparent wavelength range from 750 nm to about 275 nm followed by a sharp absorption region corresponding to an optical absorption edge of about 244 nm or 5.1 eV. The optical band gap $E_g(x)$ of $\text{Al}_x\text{Ga}_{1-x}\text{N}$ at 300K may be expressed as [15]

$$E_g(x) = E_g(\text{GaN}) (1-x) + E_g(\text{AlN}) x - b x (1-x) \\ = 3.41 (1-x) + 6.20 x - (1.0) x (1-x) \text{ eV}, \quad (4)$$

where $E_g(\text{GaN}) = 3.41 \text{ eV}$, $E_g(\text{AlN}) = 6.20 \text{ eV}$, and a bowing parameter $b = 1.0 \text{ eV}$ is assumed [14]. Using (4) and the experimentally observed band gap of 5.1 eV, one obtains $x = 0.68$ for the x-value of this particular $\text{Al}_x\text{Ga}_{1-x}\text{N}:\text{Si}$ base layer.

Figure 4b shows the optical absorption spectrum obtained for one of the solar-blind photodiode structures obtained just prior to device processing. In this case, the onset of absorption is determined by the top two layers of the structure that correspond to the two low x-value layers having a total thickness of about 700 nm. It is seen from Figure 4b that the onset of absorption for the complete device is shifted to longer wavelengths as a result of these top two layers for which an absorption edge of about 280 nm or 4.4 eV is estimated. This corresponds to an $\text{Al}_x\text{Ga}_{1-x}\text{N}$ alloy x-value of $x = 0.44$. Thus, the synthesized structure of Figure 4 corresponds

closely to the idealized device structure shown in Figure 1. That is, the photodiode structure is a solar-blind device.

3.2 Solar-Blind Photodiode Characteristics

Figure 5 shows the spectral responsivity obtained for a representative solar-blind heterostructure photodiode at zero bias (photovoltaic mode). The solar-blind device exhibits a very narrow UV spectral responsivity band peaked at 273 nm, well within the 240 - 285 nm solar blind window, with a FWHM = 21 nm. The maximum responsivity $R = 0.051$ A/W at 273 nm corresponds to an internal quantum efficiency of 27%. The responsivity falls off sharply at wavelengths greater than 285 nm since the device is transparent in this wavelength region. Likewise, the responsivity becomes very small at wavelengths shorter than 240 nm due to absorption in the n-type $\text{Al}_{0.64}\text{Ga}_{0.36}\text{N}:\text{Si}$ base layer of the device. Thus, the AlGaN heterostructure that has been developed produced a narrow solar-blind responsivity band without the need for any external filters.

Figure 6 shows plots of the current-voltage (I vs V) and the dynamic resistance DV/DI vs V exhibited by the solar-blind photodiode structure of Figure 5. As seen from the figure, the dynamic resistance of this $200 \mu\text{m} \times 200 \mu\text{m}$ square mesa device peaks at about $2 \times 10^{11} \Omega$ at zero bias, corresponding to $R_0A = 8 \times 10^7 \Omega\text{-cm}^2$. Substituting this value for R_0A along with the measured responsivity R_λ into (3) yields a detectivity $D^* = 3.3 \times 10^{12} \text{cmHz}^{1/2}\text{W}^{-1}$ at 273 nm.

Figure 7 shows plots of D^* versus wavelength for a large selection of photodetectors. It is seen from this figure that the D^* value of $3.3 \times 10^{12} \text{cmHz}^{1/2}\text{W}^{-1}$ reported here for the AlGaN solar-blind heterostructure photodiode is somewhat smaller than D^* values that we have reported earlier for visible-blind nitride photodiodes which ranged up to $D^* = 6.3 \times 10^{13} \text{cmHz}^{1/2}\text{W}^{-1}$. Note however, that these initial solar-blind AlGaN photodiodes exhibit a D^* value comparable to that of a UV-enhanced Si photodiode. However, a Si photodiode responds to radiation out to $1.1 \mu\text{m}$ — the fundamental absorption edge of Si. For a Si photodiode to respond only to radiation within the 240-285 nm solar-blind UV window, special external filters must be employed. Unfortunately, this filtering process reduces the Si solar-blind responsivity by nearly two orders of magnitude to about $D^* = 4 \times 10^{10} \text{cmHz}^{1/2}\text{W}^{-1}$. Thus, for solar-blind applications, the initial AlGaN heterostructure photodiodes reported herein are considerably more sensitive than comparable Si devices.

4 Summary and Conclusions

Backside-illuminated solar-blind UV detectors based on an AlGaN p-i-n heterostructure have been successfully synthesized, fabricated and tested. The solar-blind photodiodes exhibit a very narrow UV spectral responsivity band peaked at 273 nm with a FWHM = 21 nm. Maximum responsivity $R = 0.051$ A/W at 273 nm, corresponding to an internal quantum efficiency of 27%. R_0A values up to $8 \times 10^7 \Omega\text{-cm}^2$ were obtained, corresponding to $D^* = 3.3 \times 10^{12} \text{cmHz}^{1/2}\text{W}^{-1}$ at 273 nm.

It should be noted that these initial solar-blind AlGaN heterostructure photodiodes have very large dislocation densities — estimated to be well over 10^{10} per cm^3 . As a consequence, through dislocation reduction and continued optimization of the properties of the various device layers, one can expect substantial future improvement in the detectivity — a measure of the device sensitivity. D^* values of $10^{14} \text{cmHz}^{1/2}\text{W}^{-1}$ (or even $10^{15} \text{cmHz}^{1/2}\text{W}^{-1}$) may eventually be achievable for solar-blind detectors based on AlGaN heterostructure photodiodes.

ACKNOWLEDGMENTS

The work at NCSU is being supported by Defense Advanced Research Projects Agency grant DAAD19-99-0010 under the Solar Blind Detector Program directed by Dr. E. Martinez.

REFERENCES

- [1] C. E. Kolb, S. B. Ryali, J. C. Wormhoudt, *SPIE Proc.* **932**, 2 (1988).
- [2] Hadis Morkoc, *Nav. Res. Rev.* **51**, 26 (1999).
- [3] Dennis K. Wickenden, Zhenchun Huang, D. Brent Mott, Peter K. Shu, *Johns Hopkins APL Tech. Dig.* **18**, 217 (1997).
- [4] Wei Yang, Thomas Novova, Subash Krishnankutty, Robert Torreano, Scott McPherson, Holly Marsh, *Appl. Phys. Lett.* **73**, 1086 (1998).
- [5] T. Huang, D. B. Mott, A. La, *SPIE Proc.* **3765**, 254 (1999).
- [6] J.D. Brown, Zhonghai Yu, J. Matthews, S. Harney, J. Boney, J.F. Schetzina, J.D. Benson, K.W. Dang, C. Terrill, Thomas Nohava, Wei Yang, Subash Krishnankutty, *MRS Internet J. Nitride Semicond. Res.* **4**, 9 (1999).
- [7] J. D. Brown, J. Matthews, S. Harney, J. C. Boney, J. F. Schetzina, J. D. Benson, K. V. Dang, Thomas Nohava, Wei Yang, Subash Krishnankutty, *MRS Internet J. Nitride Semicond. Res.* **5S1**, W1.9 (2000).
- [8] J.D. Brown, J. Boney, J. Matthews, P. Srinivasan, J.F. Schetzina, Thomas Nohava, Wei Yang, Subash Krishnankutty, *MRS Internet J. Nitride Semicond. Res.* **5**, 6 (2000).
- [9] D. Walker, V. Jumar, K. Mi, P. Kung, X. H. Zhang, M. Razeghi, *Appl. Phys. Lett.* **76**, 403 (2000).

- [10] E. L. Tarsa, P. Kozodoy, J. Ibbetson, B. P. Keller, *Appl. Phys. Lett.* **77**, 316 (2000).
- [11] S.L. Chuang, *Physics of Optoelectronic Devices*, (Wiley, New York, 1995), .
- [12] J. W. Huang, T. F. Kuech, H. Lu, I. Bhat, *Appl. Phys. Lett.* **68**, 2392 (1996).
- [13] E. Schibli, A. G. Milnes, *Sol. St. Electr.* **11**, 323 (1968).
- [14] Shuji Nakamura, Gerhard Fasol, *The Blue Laser Diode - GaN based Light Emitters and Lasers*, (Springer-Verlag, Heidelberg, 1997), .
- [15] Y. Koide, H. Itoh, M. R. H. Khan, K. Hiramatu, N. Sawaki, I. Akasaki, *J. Appl. Phys.* **61**, 4540-4543 (1987).

FIGURES

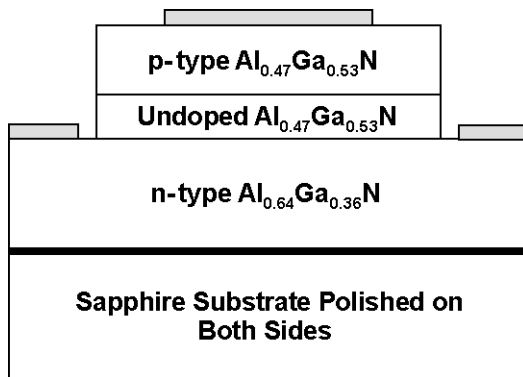


Figure 1. Schematic of AlGaN p-i-n photodiode structure.

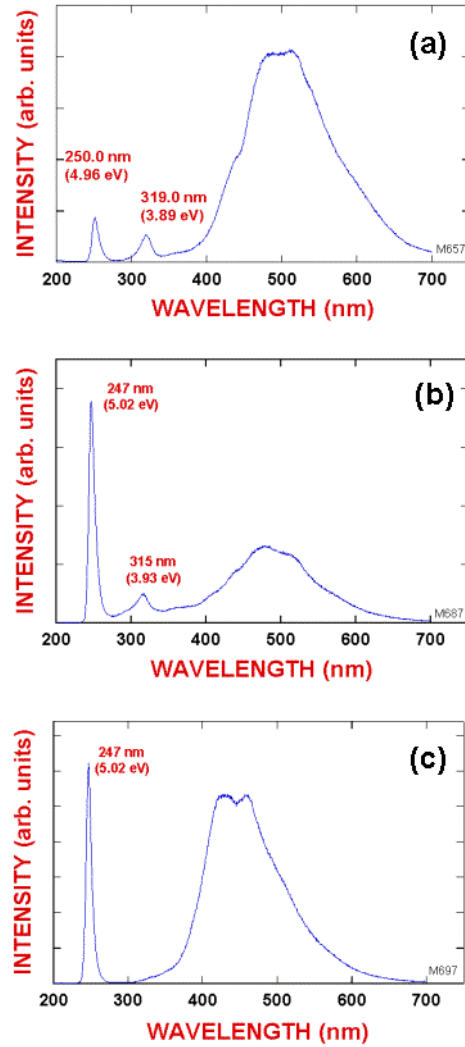


Figure 2. Cathodoluminescence spectra for n-type AlGaN:Si layers grown under different conditions.

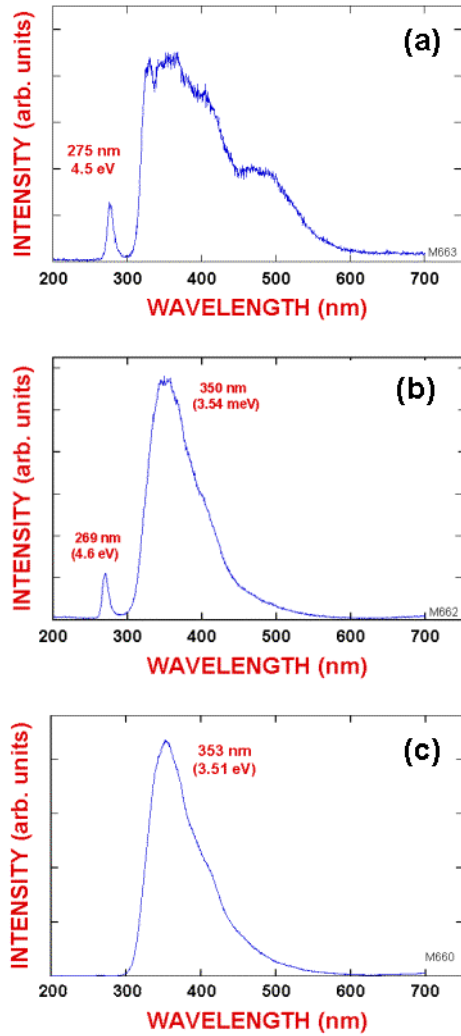


Figure 3. Cathodoluminescence spectra for three AlGaIn:Mg layers having different dopant levels.

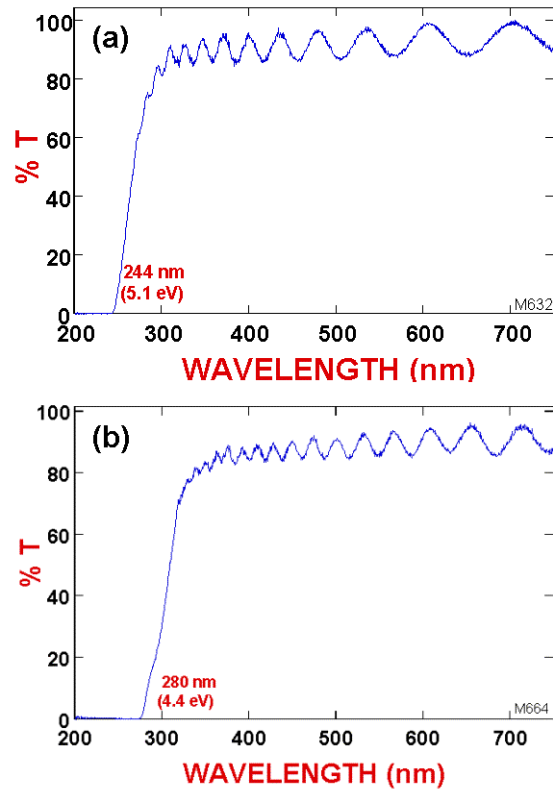


Figure 4. Optical transmittance through (a) AlGaIn n-type base layer, (b) entire solar-blind heterostructure photodiode.

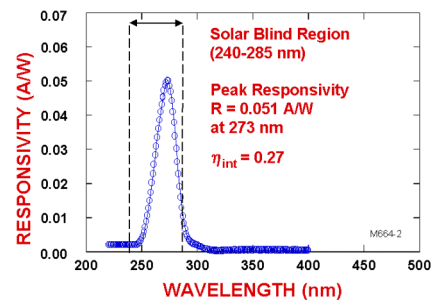


Figure 5. Spectral responsivity spectrum for solar-blind AlGaIn heterostructure photodiode. Responsivity peak occurs at 273 nm with a FWHM = 21 nm.

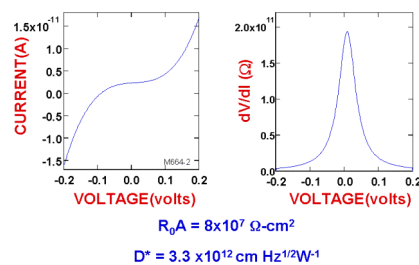


Figure 6. Electrical characteristics of solar-blind AlGaIn heterostructure photodiode.

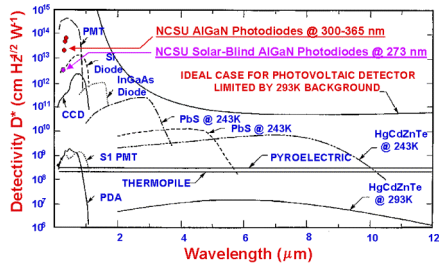


Figure 7. Detectivity versus wavelength for selected photodetectors.